SPACE DEBRIS PHYSICS AND LASER RADIOMETRIC SENSING

J. I. Peltoniemi, N. Zubko, J. Näränen, A. Raja-Halli, N. Kareinen, A. Virkki, R. Vantola, J. Eskelinen, and H. Koivula

FGI, Email: {jouni.peltoniemi, nataliya.zubko, jyri.naranen, arttu.raja-halli, anne.virkki, niko.kareinen, joona.eskelinen, renne.vantola, hannu.koivula}@nls.fi

ABSTRACT

We are developing physical models for space debris and their interactions with light and other electromagnetic radiation, including scattering, absorption, and radiation pressure. We are developing inverse techniques to derive target properties from light scattering data that we measure at our laboratory in Otaniemi, Finland. In addition, we are developing novel sensor concepts for space debris observation and characterization by numerical simulations. We are also developing concepts to manipulate the orbital objects by laser light.

We are enhancing our laboratory setup, to allow us to measure the full light scattering matrix of space debris analogues, as a function of 3 angles. That is, we will be able to illuminate and view debris analogues over full 3D space. This allows us to reproduce full light, phase, and polarisation curves. In the recent past, we have been validating the scattering and inversion models. When the laboratory is completed, we will start evaluating experimentally many novel ground- and space bases sensor and momentum transfer concepts.

Keywords: LaTeX; ESA; macros.

1. INTRODUCTION

The space debris problem is growing. Collision risks are increasing. It is estimated that there are over 1 million objects of over 1 cm in size that can be hazardous to space craft in Earth orbit [1, 2]. Only some 40 000 of these are catalogued, but many orbits are still too uncertain for effective collision avoidance.

Current sensors to measure the space debris are still too few to monitor even a fraction of the objects, and limited to larger sizes. Typically, lasers, telescopes, and radars used for measurements are based on legacy geodetic, astronomical, and military sensors, and are not necessarily most optimal for SST and space debris. We do here some theoretical and experimental studies on some novel concepts for ground and space based laser instruments to detect and identify more unknown space debris particles.

We previously developed scattering and remote sensing models for planets, vegetation, and snow[3, 4, 5]. We started modelling space debris within an ESA funded ”In Orbit Laser Momentum Transfer” project[6, 7], with Thales Alenia Space, FR. We continued in an ESA project ”Coincident orbital laser sheet particle monitoring”, where we developed simulations and laser techniques more with CSEM, CH.

2. SPACE DEBRIS MODEL

We are developing a physical model for small space debris particles, based on laboratory data and various assumptions[8]. Currently, the model has three base shapes

- Diskuloid is a round edged disk or elliptic spherocylinder,
- Ellipsoid, aspect ratio 0.5–2,
- Capsuloid is a round ended elliptic capsule or prolate spherocylinder,

each parametrized with three axis and two surface roughness parameters. This is close the the shape model in ORDEM 4.0, but our model has rounded sides and ends of the cylinder and possibly different roughness (Alyssa et al, THIS CONFERENCE). This far, materials include metal, carbon fibre reinforced polymer (CFRP), plastics, mineral, paint. Each object can further have dust on the surface or turbidity inside, modelled as volume scattering. More complex shapes, such as angled rods or bent plates, are built from these. Cubic forms are still under construction.

We computed and tabulated the scattering from a test set of 11 basic types and a few subtypes of different aspect ratio or roughness.

The model is designed for a size range from 1 mm to 10 cm. However, for this study, to be able to demonstrate some new ideas, we extrapolate up to 2 m sizes. The upper range already lacks many debris types and features,

Proc. 9th European Conference on Space Debris, Bonn, Germany, 1–4 April 2025, published by the ESA Space Debris Office
Editors: S. Lemmens, T. Flohrer & F. Schmitz, (http://conference.sdo.esoc.esa.int, April 2025)

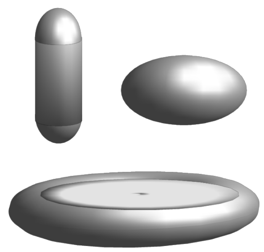

Figure 1. The current basic shapes in the model: capsuloid, ellipsoid, and diskuloid. More complex shapes built of these. To be completed with cubic shapes soon.

but can still be better than anything else, e.g. the plain link equation.

We have built a 3D table linking our model particles to MASTER source classes[1, 9], at different sizes, Table1, making use of data from many important experiments[10, 11, 12, 13, 14, 15, 16]. Thus, using the MASTER as input, we can provide spatial distributions also for our model particles, to be used in simulations. The MASTER classes are EXPL = Explosion Fragments, COLL = Collision fragments, LMRO = Launch/Mis, NAKD = NaK-Droplets, SRMS = Solid rocket motor slag, SRMD = Solid rocket motor dust, PAFL = Paint Flakes, EJEC = Ejecta, MLI = multi layer insulation, C1 = Cloud 1, C2 = Cloud 2, C3 = Cloud 3, C4 = Cloud 4, C5 = Cloud 5, MAN = all man-made, MTBG = Meteoroidal background, Streams, TOT = Total. (This may be becoming obsolete with the more detailed shape models in ORDEM 4.0 and next MASTER update (Andre, THIS MEETING).)

3. INVERSION

We work on several inversion models to retrieve size, shape, and material properties from measurement data. For this presentation, we have used simple brute force technique running over all tabulated particle types, sizes, and orientations, with interpolation and extrapolation, where needed. This may be sufficient for test runs and statistical analysis, but every real particle is individual, and one may want to extract more details. Thus, we are studying traditional light curve inversion techniques with assumed surface scattering and parametrized convex shape (triangulation or spherical harmonics), to retrieve more detailed shape and rotation, in another Mexican-Finnish collaboration [17].

4. SIMULATIONS

We have previously simulated many space based laser measurements concept using dual laser sheet system or wide angle lidars with a camera system counting all particles hitting the beam. The simulator generates a stream of particles, based on the MASTER distribution and FGI model types, passing the sensor range, illuminates with the laser beam, models the scattering, emulates the camera image, adds some random noise and disturbances, and inverts the data set.

Since the monolithic satellites had limited performance, we extended the concept to a small swarm of satellites, one transmitting a long laser beam, and the other ones circling around the beam and imaging the flashes of any particle passing the beam. One beam can actually support even hundreds of cubesat sized detectors, or the swarm could piggy-pack any laser beam for whatever purpose, e.g. communication, ranging.

Further, we have now extended the simulator to ground based laser measurements. We are making numerical experiments with several multi-directional concepts, with multiple receivers and/or transmitters at different locations, with and without polarisation, shorter and longer baselines.

Here, we demonstrate the simulation capacity with three times four concepts. First, using traditional 60 cm telescopes and moderate 10 W lasers that can be bought almost off the shelf. Next, To make the sensor system better detect our space debris model particles below 10 cm in size, we assume a largest currently operating liquid mirror telescope of a diameter of 4 m [18], and almost available laser of 500 W in mean power. Finally, we extrapolate the telescope size to 9 m, and laser power to 10 kW, that could still be technically possible by scaling or multiplying things up. We assume the first sensor setup to just survey the sky, and then trigger a more powerful and/or narrower pulse or burst to the target. We the study two geometry — basic mono static system and multi-static system of 7 receivers in random location inside a circle of a radius of 200 km — and two polarisation setup: unpolarised and circularly polarised.

5. SAMPLES

We have a collection of space debris analogue samples received from Fraunhofer Institute and some own production. The set contains mostly CFRP needles, plates, and thin aluminium pieces from solar cells, of size range 1-30 mm (Fig. 2). This allows preliminary model validation.

Particle class	EXPL	COLL	LMRO	NAKD	SRMS	SRMD	PAFL	EJEC	MLI	C 1	C 2	C 3	C 4	C 5	MAN	MTBG	Streams	TOT	size [m]
Carbon needle	0.0	0.0	0.0	0.0	0.0	0.0	0.0	0.0	0.0	0.0	0.0	0.0	0.0	0.0	-0.0	0.0	0.0	-0.0	1
CFRP flake	0.1	0.1	0.0	0.0	0.0	0.0	0.0	0.1	0.0	0.0	0.0	0.0	0.0	0.0	-0.0	0.0	0.0	-0.0	1
CFRP needle	0.0	0.0	0.0	0.0	0.0	0.0	0.0	0.0	0.0	0.0	0.0	0.0	0.0	0.0	-0.0	0.0	0.0	-0.0	1
Plastics	0.1	0.1	0.0	0.0	0.0	0.0	0.0	0.0	0.8	0.0	0.0	0.0	0.0	0.0	-0.0	0.0	0.0	-0.0	1
Paintflake	0.0	0.0	0.0	0.0	0.0	0.0	1.0	0.0	0.0	0.0	0.0	0.0	0.0	0.0	-0.0	0.0	0.0	-0.0	1
Metal rod	0.5	0.5	0.0	0.0	0.0	0.0	0.0	0.0	0.0	0.0	0.0	0.0	0.0	0.0	-0.0	0.0	0.0	-0.0	1
Metal plate	0.1	0.1	0.0	0.0	0.0	0.0	0.0	0.3	0.2	0.0	0.0	0.0	0.0	0.0	-0.0	0.0	0.0	-0.0	1
Metal droplet	0.0	0.0	0.0	1.0	0.0	0.0	0.0	0.1	0.0	0.0	0.0	0.0	0.0	0.0	-0.0	0.0	0.0	-0.0	1
Metal messy	0.2	0.2	0.0	0.0	0.0	0.0	0.0	0.4	0.0	0.0	0.0	0.0	0.0	0.0	-0.0	0.0	0.0	-0.0	1
Mineral grain	0.0	0.0	0.0	0.0	0.0	0.0	0.0	0.0	0.0	0.0	0.0	0.0	0.0	0.0	-0.0	0.8	0.0	-0.0	1
Metal grain	0.0	0.0	0.0	0.0	0.0	0.0	0.0	0.1	0.0	0.0	0.0	0.0	0.0	0.0	-0.0	0.2	0.0	-0.0	1
Carbon needle	0.0	0.0	0.0	0.0	0.0	0.0	0.0	0.0	0.0	0.0	0.0	0.0	0.0	0.0	-0.0	0.0	0.0	-0.0	0.1
CFRP flake	0.1	0.1	0.0	0.0	0.0	0.0	0.0	0.1	0.0	0.0	0.0	0.0	0.0	0.0	-0.0	0.0	0.0	-0.0	0.1
CFRP needle	0.1	0.1	0.0	0.0	0.0	0.0	0.0	0.4	0.0	0.0	0.0	0.0	0.0	0.0	-0.0	0.0	0.0	-0.0	0.1
Plastics	0.05	0.05	0.0	0.0	0.0	0.0	0.0	0.0	0.8	0.0	0.0	0.0	0.0	0.0	-0.0	0.0	0.0	-0.0	0.1
Paint flake	0.0	0.0	0.0	0.0	0.0	0.0	1.0	0.0	0.0	0.0	0.0	0.0	0.0	0.0	-0.0	0.0	0.0	-0.0	0.1
Metal rod	0.5	0.5	0.0	0.0	0.0	0.0	0.0	0.0	0.0	0.0	0.0	0.0	0.0	0.0	-0.0	0.0	0.0	-0.0	0.1
Metal plate	0.05	0.05	0.0	0.0	0.0	0.0	0.0	0.3	0.2	0.0	0.0	0.0	0.0	0.0	-0.0	0.0	0.0	-0.0	0.1
Metal droplet	0.0	0.0	0.0	1.0	0.0	0.0	0.0	0.1	0.0	0.0	0.0	0.0	0.0	0.0	-0.0	0.0	0.0	-0.0	0.1
Metal messy	0.2	0.2	0.0	0.0	0.0	0.0	0.0	0.0	0.0	0.0	0.0	0.0	0.0	0.0	-0.0	0.0	0.0	-0.0	0.1
Mineral grain	0.0	0.0	0.0	0.0	0.0	0.0	0.0	0.0	0.0	0.0	0.0	0.0	0.0	0.0	-0.0	0.8	0.0	-0.0	0.1
Metal grain	0.0	0.0	0.0	0.0	0.0	0.0	0.0	0.1	0.0	0.0	0.0	0.0	0.0	0.0	-0.0	0.2	0.0	-0.0	0.1
Carbon needle	0.0	0.0	0.0	0.0	0.0	0.0	0.0	0.0	0.0	0.0	0.0	0.0	0.0	0.0	-0.0	0.0	0.0	-0.0	0.01
CFRP flake	0.15	0.15	0.0	0.0	0.0	0.0	0.0	0.1	0.0	0.0	0.0	0.0	0.0	0.0	-0.0	0.0	0.0	-0.0	0.01
CFRP needle	0.2	0.2	0.0	0.0	0.0	0.0	0.0	0.5	0.0	0.0	0.0	0.0	0.0	0.0	-0.0	0.0	0.0	-0.0	0.01
Plastics	0.05	0.05	0.0	0.0	0.0	0.0	0.0	0.0	0.8	0.0	0.0	0.0	0.0	0.0	-0.0	0.0	0.0	-0.0	0.01
Paint flake	0.0	0.0	0.0	0.0	0.0	0.0	1.0	0.0	0.0	0.0	0.0	0.0	0.0	0.0	-0.0	0.0	0.0	-0.0	0.01
Metal rod	0.5	0.5	0.0	0.0	0.0	0.0	0.0	0.0	0.0	0.0	0.0	0.0	0.0	0.0	-0.0	0.0	0.0	-0.0	0.01
Metal plate	0.05	0.05	0.0	0.0	0.0	0.0	0.0	0.5	0.2	0.0	0.0	0.0	0.0	0.0	-0.0	0.0	0.0	-0.0	0.01
Metal droplet	0.0	0.0	0.0	1.0	0.0	0.0	0.0	0.1	0.0	0.0	0.0	0.0	0.0	0.0	-0.0	0.0	0.0	-0.0	0.01
Metal messy	0.05	0.05	0.0	0.0	0.0	0.0	0.0	0.0	0.0	0.0	0.0	0.0	0.0	0.0	-0.0	0.0	0.0	-0.0	0.01
Mineral grain	0.0	0.0	0.0	0.0	0.0	0.0	0.0	0.0	0.0	0.0	0.0	0.0	0.0	0.0	-0.0	0.8	0.0	-0.0	0.01
Metal grain	0.0	0.0	0.0	0.0	0.0	0.0	0.0	0.1	0.0	0.0	0.0	0.0	0.0	0.0	-0.0	0.2	0.0	-0.0	0.01
Carbon needle	0.0	0.0	0.0	0.0	0.0	0.0	0.0	0.0	0.0	0.0	0.0	0.0	0.0	0.0	-0.0	0.0	0.0	-0.0	0.001
CFRP flake	0.2	0.2	0.0	0.0	0.0	0.0	0.0	0.1	0.0	0.0	0.0	0.0	0.0	0.0	-0.0	0.0	0.0	-0.0	0.001
CFRP needle	0.6	0.6	0.0	0.0	0.0	0.0	0.0	0.5	0.0	0.0	0.0	0.0	0.0	0.0	-0.0	0.0	0.0	-0.0	0.001
Plastics	0.05	0.05	0.0	0.0	0.0	0.0	0.0	0.0	0.8	0.0	0.0	0.0	0.0	0.0	-0.0	0.0	0.0	-0.0	0.001
Paint flake	0.0	0.0	0.0	0.0	0.0	0.0	1.0	0.0	0.0	0.0	0.0	0.0	0.0	0.0	-0.0	0.0	0.0	-0.0	0.001
Metal rod	0.05	0.05	0.0	0.0	0.0	0.0	0.0	0.0	0.0	0.0	0.0	0.0	0.0	0.0	-0.0	0.0	0.0	-0.0	0.001
Metal plate	0.05	0.05	0.0	0.0	0.0	0.0	0.0	0.1	0.2	0.0	0.0	0.0	0.0	0.0	-0.0	0.0	0.0	-0.0	0.001
Metal droplet	0.0	0.0	0.0	1.0	0.0	0.0	0.0	0.1	0.0	0.0	0.0	0.0	0.0	0.0	-0.0	0.0	0.0	-0.0	0.001
Metal messy	0.05	0.05	0.0	0.0	0.0	0.0	0.0	0.0	0.0	0.0	0.0	0.0	0.0	0.0	-0.0	0.0	0.0	-0.0	0.001
Mineral grain	0.0	0.0	0.0	0.0	0.0	0.0	0.0	0.0	0.0	0.0	0.0	0.0	0.0	0.0	-0.0	0.8	0.0	-0.0	0.001
Metal grain	0.0	0.0	0.0	0.0	0.0	0.0	0.0	0.1	0.0	0.0	0.0	0.0	0.0	0.0	-0.0	0.2	0.0	-0.0	0.001
Carbon needle	0.4	0.4	0.0	0.0	0.0	0.0	0.0	0.5	0.0	0.0	0.0	0.0	0.0	0.0	-0.0	0.0	0.0	-0.0	0.0001
CFRP flake	0.1	0.1	0.0	0.0	0.0	0.0	0.0	0.1	0.0	0.0	0.0	0.0	0.0	0.0	-0.0	0.0	0.0	-0.0	0.0001
CFRP needle	0.3	0.3	0.0	0.0	0.0	0.0	0.0	0.3	0.0	0.0	0.0	0.0	0.0	0.0	-0.0	0.0	0.0	-0.0	0.0001
Plastics	0.05	0.05	0.0	0.0	0.0	0.0	0.0	0.0	0.8	0.0	0.0	0.0	0.0	0.0	-0.0	0.0	0.0	-0.0	0.0001
Paint flake	0.0	0.0	0.0	0.0	0.0	0.0	1.0	0.0	0.0	0.0	0.0	0.0	0.0	0.0	-0.0	0.0	0.0	-0.0	0.0001
Metal rod	0.05	0.05	0.0	0.0	0.0	0.0	0.0	0.0	0.0	0.0	0.0	0.0	0.0	0.0	-0.0	0.0	0.0	-0.0	0.0001
Metal plate	0.05	0.05	0.0	0.0	0.0	0.0	0.0	0.05	0.2	0.0	0.0	0.0	0.0	0.0	-0.0	0.0	0.0	-0.0	0.0001
Metal droplet	0.0	0.0	0.0	1.0	0.0	0.0	0.0	0.0	0.0	0.0	0.0	0.0	0.0	0.0	-0.0	0.0	0.0	-0.0	0.0001
Metal messy	0.0	0.0	0.0	0.0	0.0	0.0	0.0	0.0	0.0	0.0	0.0	0.0	0.0	0.0	-0.0	0.0	0.0	-0.0	0.0001
Mineral grain	0.0	0.0	0.0	0.0	0.0	0.0	0.0	0.0	0.0	0.0	0.0	0.0	0.0	0.0	-0.0	0.8	0.0	-0.0	0.0001
Metal grain	0.05	0.05	0.0	0.0	0.0	0.0	0.0	0.05	0.0	0.0	0.0	0.0	0.0	0.0	-0.0	0.2	0.0	-0.0	0.0001

Table 1. Fractional amounts of various particle types in MASTER classes vs. the FGI scattering model.

Figure 2. Some samples

6. LABORATORY

The laboratory has a flexible goniometer system that allows 3-axis rotation, e.g. azimuth, zenith, and target angles. One can build a hemispherical construction for surface reflectance measurements, or (almost) full spherical for single particle scattering measurements. The measurement angles can be selected freely using a list of values.

Currently, the main detector is an ASD FieldSpec 4 spectroradiometer, working in a wavelength range of 350 – 2500 nm. The fore optics can be tuned for selected field of view, from 1 cm to 10 cm. There is an option for full polarisation measurements, using a rotating wire grid polariser and adjustable LCD retarder. The ASD is, however, not the most ideal sensor here, because of some internal polarisation dependence, the heterogeneous light cable input, dependence on the cable movements, low sensitivity, high noise, and some strange low light features. Thus, new detectors are needed, but currently we must use what is available.

For illumination, two quartz tungsten halogen (QTH) sources from Oriel are available, with powers of 200 and 1000 W, providing broadband light in visual and short wave infrared (SWIR). The 200 W source can be used with a liquid light guide that smoothens the filament features and produces 5–10 cm quasi-homogeneous spot. The bigger one can make a spot diameter of 10 – 50 cm. The incident light can also be polarised using similar wire grid and rotator, though this eats brightness even more than the 50% by the polariser, because of more complicated optical path.

The sample can be positioned on a sample tray, on a post and needle, or hanging by a spider web (Fig. 5). Other levitation options are being studied.

The measurements are calibrated using a Spectralon cylinder by Labsphere (originally a filling for the holes in an integrating sphere), Fig. 6. Dark current is measured before every set, and subtracted from the raw number, based on a formula in the ASD manual, but noting a sign error there that corrupted some of our previous measurements.

The system is steered using a python script in a Raspberry Pi 3 computer.

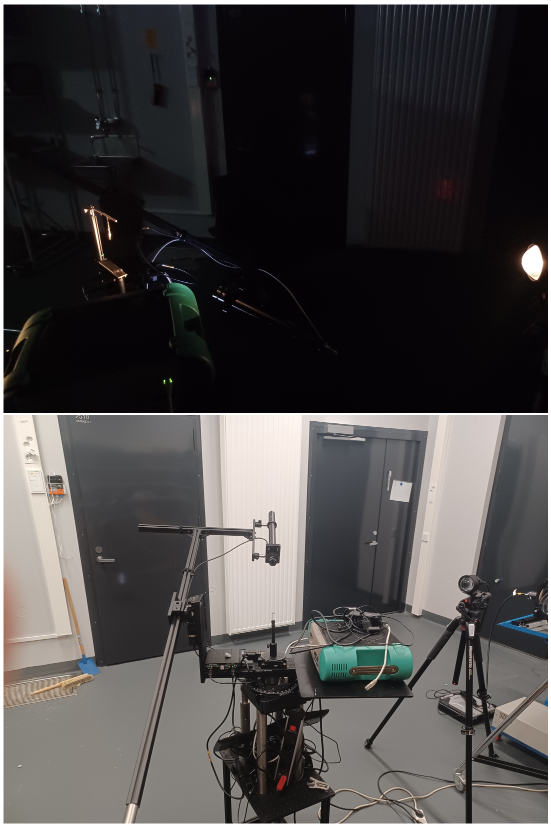

Figure 3. The gonioradiometer in action and after action. The light source is on the right, the green-grey box is the ASD FieldSpec 4 spectroradiometer, the fore optics with the rotating polariser is on the arm, and three rotating motors with their controllers in the centre.

7. RESULTS

We show here a couple of sample results from modelling, measurements, and simulations. Fig. 7 compares the modelled and measured scattering as a function of the phase and azimuth angles, for three samples: CFRP needle, metal plate, and rolled piece of reflecting multi-layer insulation (MLI). The phase angle is extended to negative values for azimuths $> 180°$, thus there are totally 6 azimuth angles shown. One can note that the model and measurements follow same pattern, though there are some differences, because the target is more complex than the model. The dependence on the two angles is strong. Because the target is inclined against the beam there is azimuthal asymmetry. The three samples have quite differing features, especially at larger phase angles, but near backscattering it may be more challenging to distinguish them. The CFRP seems to polarise strongest, and the metal plate weakest, but better signal to noise ratio is needed for more advanced analysis. By tuning the surface roughness and impurities, one could improve the fit for individual samples.

We compare the four geometric-polarised setups in Table 2. The unpolarised mono-static system performed as

Figure 4. The light sources. 1000 W Oriel QTH on the top, the 200 W QTH in the background, connected to the lamp optics on the left with a liquid light cable.

Figure 5. A CFRP needle hanging in a spider web.

well as a random guess in identification, and size error was also very large. With polarisation, the identification improved to about 70%, which is rather a good number, and size error also decreased. Multi-static setup helped only little in identification, probably due to too narrow angular range. Multi-static polarised gave best size, but still not too impressive. Multi-static transmission with many lasers failed this far, because of precision problems in pointing, even in simulations. Light curve (time series of a rotating body) should bring additional information on shapes, one snapshot alone is limited.

In Table 3 we further compare, how many MASTER particles a zenith-looking laser telescope could find. With a typical 60 cm telescope and moderate 10 W laser, one might be lucky to detect even few particles a year. Using 500 W laser power and 4 m liquid mirror telescope, one could already detect hundreds of objects, which might be close to make demonstrations. The largest setup that

Figure 6. The Labsphere Spectralon cylinder used as a calibration target.

system	identified	relative size error
2I	10%	6.0
2V, circularly polarised	70%	2.0
7I, multi-static	20%	5.0
7V both	70%	1.0

Table 2. The fraction of correctly identified samples from all test set, and the error in the relative size.

could be still almost possible with 9 m telescope and 10 kW laser power detects already thousands or even tens of thousands of new and old objects, and could be a useful operational sensor. Of course, with any preinformation of directions, e.g. towards a known cloud of debris, or triggered by optical telescopes or radars, the numbers can be very much larger. The numbers may also be smaller, if we cannot meet the optimistic assumptions of sensor noise, sensitivity, resolution, clean atmosphere, and laser bandwidth. Also, uncertainties and misinterpretations with the MASTER data reflect directly here.

system	dets/s	dets/year
60 cm, 10 W	2E-7	5
4 m, 500 W	1.5E-5	400
9 m, 10 kW	0.0008	20 000

Table 3. The detection rate of space debris passing a laser beam at different configurations, given as per second and per ideal year without any interruptions.

8. CONCLUSIONS

We are developing advanced model for the optical, electromagnetic, morphological properties of space debris. The measurements help the model to converge towards realistic predictions, though many gaps and discrepancies remain.

The space gonioradiometer system works basically nicely, but for precise measurements of small debris particles, the signal remains low and noisy, especially with polarisation. Ideal target size for the current setup would

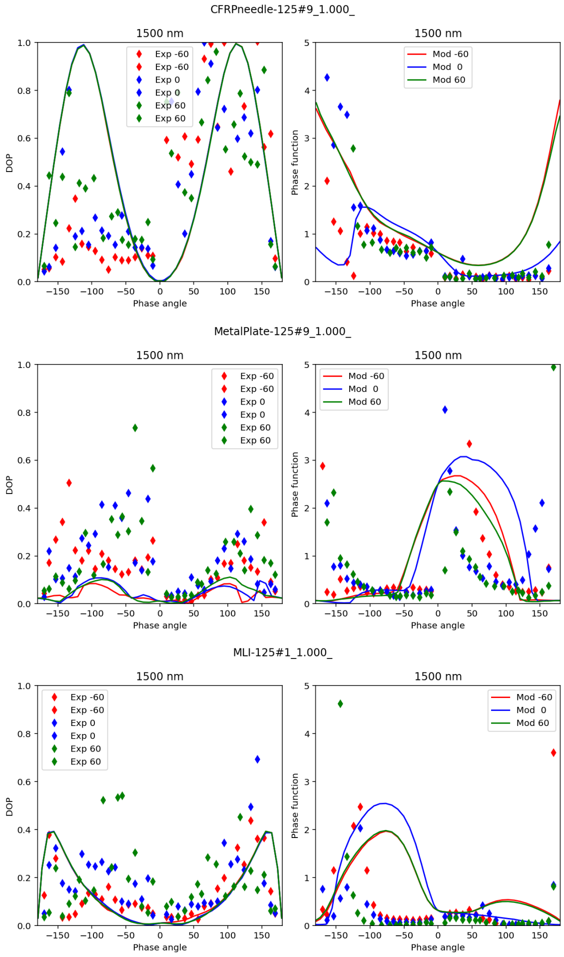

Figure 7. The scattering phase function (right) and degree of linear polarisation (left) of a CFRP needle, a metal plate, and a roll of MLI as a function of the phase angle and 6 azimuths (symbols + negative phase angles).

be 2–5 cm. For smaller objects, a stronger light source or more sensitive detector is needed, probably using lasers.

Typically, the debris particles have strong angular signal of the rotation, phase angle, and azimuth. This depends dominantly on the shape, and thus allows recovering some shape information from the light or phase curves. However, it can be a small challenge to get sufficiently wide angular range from ground based multistatic measurements. Preliminarily, based on models and a few noisy measurements, the debris particles polarise and depolarise more or less strongly, depending on the material, size, and surface structure, allowing potentially also some inversion. Due to a low number of samples and low signal, we cannot say yet too much about spectral signals, but there can be some trends to study more.

The large zenith telescope system provided exciting numbers, but there are too many open issues to make any promises. Depending on, how low the noise can be dropped, the system could detect thousands of new debris objects or lost satellites a year, track almost all known LEO–GEO satellites in view, and even get a signal from the Moon and some passing NEOs, notably 99942 Apophis at year 2029 and 2024YR4 at 2028. However, the performance could be much better, if seamlessly linked with radar or passive optical systems.

For the next steps, we consider most important to continue the experiments. We shall upgrade the laboratory to measure new samples with improved precision, to extract reference level light, phase, polarisation, and spectral curves. We shall extend the experiment to validate the proposed sensing concepts in more detail and realism in laboratory and outdoors, e.g. using the real lasers in Metsähovi horizontally in cloudy days, with close to real sensors in 100 m's baseline, varying the geometry, sensor properties, and sampling.

Further, the space debris model shall be completed with more debris types. e.g. solid rocket slag and more complex metal parts. The FGI model shall be linked more tightly with MASTER model. The simulator shall be interfaced with atmosphere tools, detailed detector properties, and high level sensor simulators.

We are optimistic to reach major progress in new space debris sensing concepts, extending to crucial 1–10 cm range, but that needs many steps in many fields, and lot of new thinking outside the old boxes.

ACKNOWLEDGMENTS

REFERENCES

1. Sven Flegel, J. Gelhaus, C. Wiedemann, P. Vörsmann, Michael Oswald, S. Stabroth, H. Klinkrad, and Holger Krag. The MASTER-2009 space debris environement model. *European Space Agency, (Special Publication) ESA SP*, 672, 2009.
2. ESA, Space Debris Office. ESA's Space Environment Report 2022.
3. J. I. Peltoniemi, M. Gritsevich, T. Hakala, P. Dagsson-Waldhauserová, Ó. Arnalds, K. Anttila, H.-R. Hannula, N. Kivekäs, H. Lihavainen, O. Meinander, J. Svensson, A. Virkkula, and G. de Leeuw. Soot on snow experiment: bidirectional reflectance factor measurements of contaminated snow. *The Cryosphere*, 9:2323–2337, 2015.
4. J. I. Peltoniemi, M. Gritsevich, J. Markkanen, T. Hakala, J. Suomalainen, N. Zubko, O. Wilkman, and K. Muinonen. A Composite Model for Reflectance and Polarisation of Light from Granulate Materials. *ISPRS Annals of Photogrammetry, Remote Sensing and Spatial Information Sciences*, V-1-2020:375–382, 2020.
5. Juha Suomalainen, Teemu Hakala, Eetu Puttonen, and Jouni Peltoniemi. Polarised bidirectional reflectance factor measurements from vegetated land

surfaces. *J. Quant. Spectrosc. Radiat. Transfer*, 110:1044–1056, 2009.

6. Damien Dumestier. Space Debris Deflection by Space Based Laser. In *8th European Conference on Space Debris*, 2021.
7. Jouni I. Peltoniemi, Olli Wilkman, Maria Gritsevich, Markku Poutanen, Arttu Raja-Halli, Jyri Näränen, Tim Flohrer, and Andrea Di Mira. Steering reflective space debris using polarised lasers. *Advances in Space Research*, 67(6):1721–1732, 2021.
8. Jouni I. Peltoniemi, Nataliya Zubko, Anne K. Virkki, Maria Gritsevich, Jarmo Moilanen, Jean-Christophe Roulet, David Nguyen, Valentin Mitev, Robin Putzar, Erkai Watson, Martin Schimmerohn, Antti Penttilä, Karri Muinonen, and Mark Millinger. Light scattering model for small space debris particles. *Advances in Space Research*, 70(10):2961–2975, November 2022.
9. *MASTER*. Published: https://sdup.esoc.esa.int/master/.
10. Samantha Allen and Norman Fitz-Coy. DebriSat fragment characterization: Quality assurance. *Journal of Space Safety Engineering*, 7(3):235–241, September 2020.
11. P. H. Krisko, M. Horstman, and M. L. Fudge. SOCIT4 collisional-breakup test data analysis: With shape and materials characterization. *Adv. Space Res.*, 41(7):1138–1146, 2008.
12. Heather Cowardin, P Seitzer, Kira Abercromby, Edwin Barker, and T. Schildknecht. Characterization of Orbital Debris Photometric Properties Derived from Laboratory-Based Measurements. page E47, September 2010.
13. Heather Cowardin, Phillip Anz-Meador, James Murray, J.-C. Liou, Eric Christiansen, Marlon Sorge, Norman Fitz-Coy, and Tom Huynh. Updates to the DebriSat Project in Support of Improving Breakup Models and Orbital Debris Risk Assessments. In *2019 15th Hypervelocity Impact Symposium*. American Society of Mechanical Engineers Digital Collection, June 2020.
14. Robin Putzar, Erkai Watson, Martin Schimmerohn, Patrik Kärräng, and Mark Millinger. How hypervelocity impacts can affect the LISA mission -The MIRAD study. In *70th International Astronautical Congress 2019At: Washington, D.C., USA*, 2019.
15. Yasuhiro Akahoshi, Pauline Faure, Haruhisa Matsumoto, and Yukihito Kitazawa. Hypervelocity Impact Tests on Ejecta and its International Stabdarization. *The Journal of Space Technology and Science*, 26(2):2_48–2_55, 2012.
16. Erkai Watson, Nico Kunert, Robin Putzar, Hans-Gerd Maas, and Stefan Hiermaier. Four-View Split-Image Fragment Tracking in Hypervelocity Impact Experiments. American Society of Mechanical Engineers Digital Collection, June 2020.
17. David Galeano, Jouni Peltoniemi, Rogerio Enríquez-Caldera, and José Guichard. Inversion of the light curves of space debris using simulated satellite-based observations. *Journal of Physics: Conference Series*, 2946(1):012001, January 2025. Publisher: IOP Publishing.
18. Paul Hickson, Bhavya Ailawadhi, Arun S, Monalisa Dubey, Naveen Dukiya, Sara Filali, Brajesh Kumar, Kuntal Misra, Vibhore Negi, Kumar Pranshu, Jean Surdej, and Saakshi Turakhia. Serendipitous detection of orbital debris by the International Liquid Mirror Telescope. *Journal of Space Safety Engineering*, May 2024.